INTERNATIONAL ATOMIC ENERGY AGENCY
UNITED NATIONS EDUCATIONAL, SCIENTIFIC AND CULTURAL ORGANIZATION
INTERNATIONAL CENTRE FOR THEORETICAL PHYSICS
I.C.T.P., P.O. BOX 586, 34100 TRIESTE, ITALY. CABLE: CENTRATOM TRIESTE

SMR.380/11

COLLEGE ON THEORETICAL AND EXPERIMENTAL RADIOPROPAGATION SCIENCE

6 - 24 February 1989

BASIC PHYSICS OF THE IONOSPHERE: A TUTORIAL REVIEW

H. RISHBETH

University of Southampton, U.K.

UDC 551.510.535
Indexing Terms: Ionosphere

Basic physics of the ionosphere: a tutorial review

H. RISHBETH, PhD, ScD*

SUMMARY
This paper is an exposition of the basic physics of the ionosphere, according to the present understanding. It concentrates on the large-scale ionospheric structure at heights above 100 km. Since the ionosphere depends greatly on the structure and dynamics of the neutral atmosphere from which it is formed, and on the geomagnetic field, brief descriptions of these are given. The paper then reviews the theoretical structure of the ionospheric layers and discusses the most important ionospheric phenomena. It concludes with a summary of recent progress and outstanding questions, and a bibliography for further reading.

*Rutherford Appleton Laboratory, Chilton, Didcot, Oxon OX11 0QX, and Department of Physics, University, Southampton SO9 5NH

List of Principal Symbols

$-e$ charge on electron
f radio frequency
g acceleration due to gravity
h height
j current density
k Boltzmann's constant
m particle mass
n gas concentration; layer index
p gas pressure ($p = nkT$)
t time
z reduced height (units of H)
B geomagnetic field
D diffusion coefficient
E electric field
F pressure gradient force
G Fl layer shape factor
H scale height ($H = RT/Mg$)
I radiation intensity; dip angle
K ion-drag coefficient; rate coefficient
L loss coefficient; magnetic L-value
M particle mass (a.m.u.)
N electron density (concentration)
R gas constant
T absolute temperature
U neutral air wind velocity
V ion/electron drift velocity
W vertical velocity
α square-law recombination coefficient
β linear loss coefficient
η ionizing efficiency
λ wavelength
μ viscosity coefficient
ν collision frequency
ρ mass density
σ absorption cross-section; conductivity
τ optical depth
ϕ geographic latitude
χ solar zenith angle
ω gyrofrequency
Λ magnetic latitude
Ω Earth's angular velocity
$h\nu$ photon

1 Introduction

1.1 What is the Ionosphere?

The ionosphere is defined as the part of the upper atmosphere in which free electrons are sufficiently numerous to influence the propagation of radio waves. For practical purposes it may be taken to extend in height from about 60 to 600 km, where the oxygen ions of the ionosphere give way to protons, but these are not well-defined limits. Figure 1 places the ionosphere in its context, by showing the extent of the ionospheric D, E and lower F regions alongside other features of the atmosphere up to 200 km.

Historically, the ionosphere was discovered by Marconi when he sent radio signals across the Atlantic in 1901. Soon afterwards, Kennelly and Heaviside suggested that free electric charges in the upper atmosphere could cause the reflection of radio waves, although the related idea of an atmospheric conducting layer, as the site of the currents that produce small daily variations of the geomagnetic field (Section 1.3), had originated with Gauss in 1839. Ionospheric physics really began in 1924/25 with Appleton and Barnett,[1] and Breit and Tuve,[2] whose experiments measured the height of the conducting layer and revealed its stratified nature. It was soon verified that the ionization is produced by solar ionizing radiation. Many facts about the ionosphere were known by 1940, but its physics and chemistry were not really established till the 1950s and 1960s.

The ionization in the upper atmosphere is of practical importance because of its role in radio communications. It is important scientifically because the charged particles are easier to detect experimentally than the neutral gas, and thus act as useful tracers for studying the upper atmos-

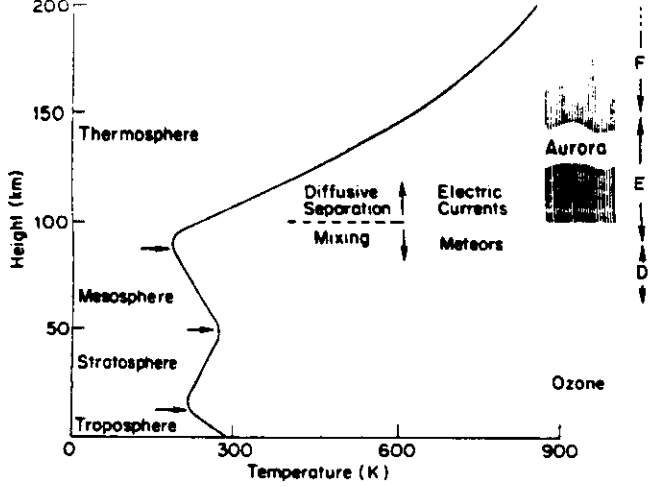

Fig. 1. Regions of the Earth's atmosphere up to 200 km, showing a typical temperature profile, the ionospheric regions D, E and the lower part of F, and heights of other features. (*Courtesy of* S.E.R.C. Rutherford Appleton Laboratory, UK)

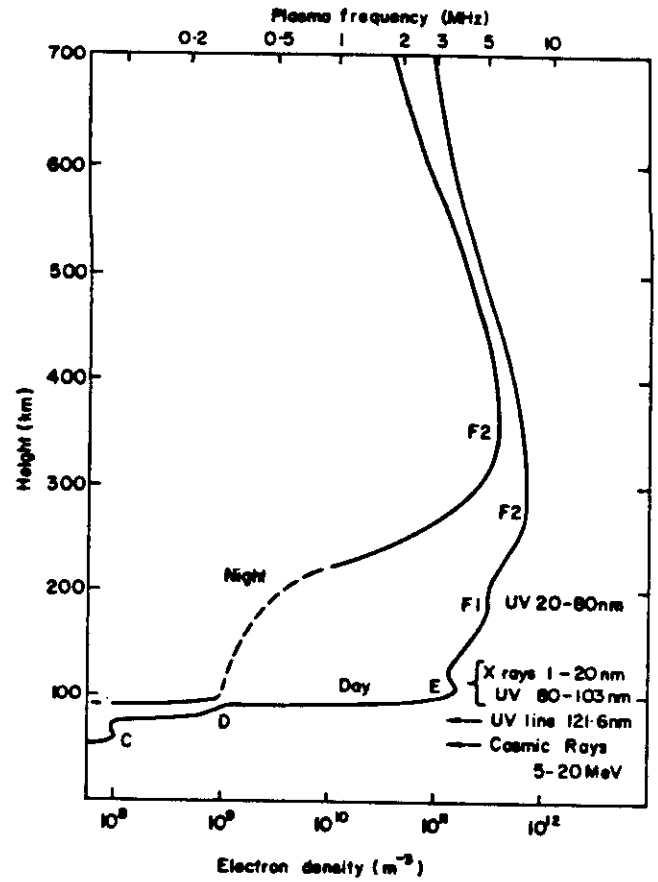

Fig. 2.. Typical mid-latitude $N(h)$ electron density profiles for moderate solar activity, showing the radiations that produce the main ionospheric layers. (From *Contemporary Physics*, **14**, p.230, 1973, Taylor & Francis, London.)

phere. But, despite its importance, the ionization is one of the minor constituents of the upper atmosphere: even in the main layers of the ionosphere, less than 1% of the air is ionized. Furthermore, the ionosphere is electrically neutral to a high degree of approximation, as positive and negative charged particles are always created and destroyed together. Even where strong electric fields exist, the charge imbalance is a minute fraction of the total charge density. The electron-ion gas of the ionosphere is a natural plasma.

This paper aims to give a very simplified survey of the ionosphere, and in particular how it depends on the neutral atmosphere and is influenced by the Earth's magnetic field. Most of the paper is devoted to well-established material, which is dealt with in greater detail in the works listed in the Bibliography. The text references are mostly to historical papers, or to general accounts of some particular topic.

1.2 Basic Physical Principles

The most important ionospheric parameter—from the point of view of radio propagation and also of the physics—is the electron density N (more correctly, the electron concentration). Typical height profiles for midlatitudes are shown in Fig. 2. Variations with height h and time t, and with latitude and longitude, can be represented either by purely descriptive empirical models, in which mathematical formulae are constructed to match the observed variations of N, or else by physical models generated by solving the theoretical continuity equation (1). More sophisticated models incorporate equations (2) and (3), for the velocities V and temperatures T of the ions and the electrons, as well as the corresponding equations for the neutral particles.

BASIC EQUATIONS FOR ANY KIND OF PARTICLE

Continuity equation (conservation of mass)

$$\partial N/\partial t = \{\text{Production}\} - \{\text{Loss}\} - \{\text{Transport}\} \quad (1)$$

Force equation (conservation of momentum)

$$d\mathbf{V}/dt = \{\text{Driving force}\} - \{\text{Drag}\} - \{\text{Advection}\}^* \quad (2)$$

Heat equation (conservation of energy)

$$\partial T/\partial t = \{\text{Heating}\} - \{\text{Cooling}\} - \{\text{Conduction}\} \quad (3)$$

1.3 The Geomagnetic Field

The behaviour of ions and electrons in the ionosphere is largely governed by the Earth's magnetic field. For many purposes this field may be represented by a dipole inclined about 12° to the Earth's axis. Consider a point on the Earth at magnetic latitude Λ, in an assumed dipole field. If the magnetic line of force (locally inclined at angle I to the horizontal) is traced outwards from the Earth, it crosses the plane of the magnetic equator at a geocentric distance of L earth radii and returns to Earth at the conjugate point at magnetic latitude $-\Lambda$, where

$$\tan I = 2 \tan \Lambda, \; L = \sec^2 \Lambda \quad (4)$$

L is termed the L-value and I the dip angle for the point in question. The dip equator, at which $I = 0°$, is 12°N of the geographic equator in India and 12°S in Peru. The dip poles, at which $I = 90°$, are in the Canadian Arctic and East Antarctica.

In low and middle latitudes (up to about $L = 6$, or $\Lambda = 66°$) the geomagnetic field lines are closed, but at higher latitudes they are linked to the magnetosphere, the tenuous region around the Earth that is permeated by the geomagnetic field. The high latitude ionosphere is profoundly affected by charged particles and electric currents, originating in the magnetosphere, that cause the aurora and magnetic storms. The particles and currents mainly enter the atmosphere in the auroral ovals, rings 2000–3000

*Advection: transport of momentum by viscosity, etc.

km in diameter that surround the magnetic poles (Section 5.7). In turn the magnetosphere is influenced by the solar wind—the stream of charged particles emitted by the Sun—and the interplanetary magnetic field. Magnetic storms tend to follow solar disturbances and the resulting strengthening of the solar wind (Section 6). During storms, the electric currents in the high latitude ionosphere may locally perturb the geomagnetic field by up to 5%, as compared to the quiet-day variations of 0·1% produced by dynamo currents in the ionosphere (Section 4.5).

The degree of geomagnetic disturbance is characterized by 'planetary geomagnetic indices' (*Ap* and *Kp*), which are computed for every 3 hours of Universal Time from records made at several magnetic observatories. *Ap* is roughly proportional to the amplitude of geomagnetic disturbance; the *Kp* index is computed on a logarithmic scale of 0–9.

1.4 Experimental Techniques for Studying the Ionosphere

This section lists the principal techniques, but does not try to explain or evaluate them in any detail. The notes are therefore very condensed and require many qualifications.

Radio probing of the ionosphere[3-4-5]

Total Reflection at the plasma frequency $f_0 = \sqrt{(80{\cdot}6N)}$ (typically HF, MF, LF in daytime F,E,D layers respectively). This is used for routine sounding of the ionosphere. It is not possible to observe above the F2 peak, except by 'topside sounders' carried in satellites. The reflection process is complicated by the geomagnetic field. See Fig. 3.

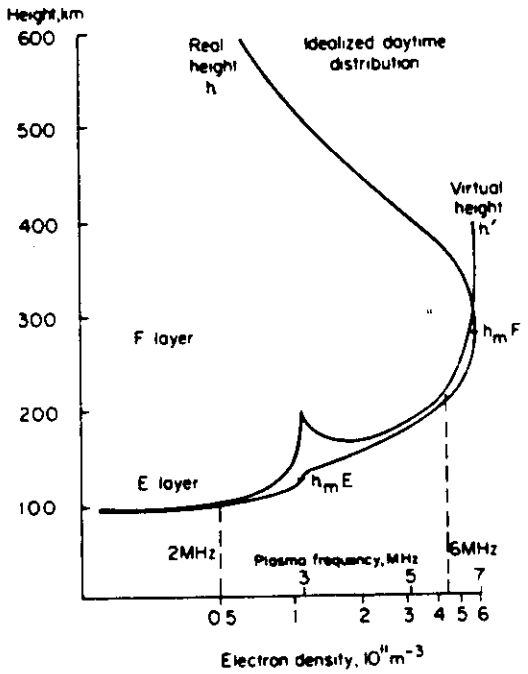

Fig. 3. Idealized ionogram obtained by an ionosonde, with the corresponding real-height $N(h)$ profile of electron density. The ionogram is a measure of 'virtual height', which corresponds to the time of travel of the radio pulse. Near the peak of a layer, the pulse is retarded and the virtual height is significantly greater than the real height, producing a 'cusp' on the ionogram, as shown. (*Courtesy of* S.E.R.C. Rutherford Appleton Laboratory).

Coherent Scatter at frequencies $\gg f_0$ (HF, VHF, UHF). Scattering occurs at (generally magnetically field-aligned) irregularities of size $\lambda/2$ (where λ = radar wavelength), as found in the auroral oval and near the magnetic equator; also from meteor trails. Velocity is measured by the Doppler effect.

Incoherent Scatter at frequencies $\gg f_0$ (VHF, UHF). Scattering from thermal random irregularities (ion-acoustic waves) of scale size $\lambda/2$. This effect is weak (depending on electron cross-section, $10^{-28}m^2$; target area typically 1 cm^2). Ion density, ion and electron temperatures, ion drift velocity, and indirectly some neutral atmosphere parameters can be measured. See Fig. 4.

Active remote sensing with man-made signals traversing the ionosphere

(a) Radio phase and polarization (Faraday rotation)
(b) LF, VLF reflection, MF partial reflection in the lower ionosphere
(c) Radio wave absorption (signal strength)
(d) Radar studies of meteor echoes (neutral air density and winds)

Passive remote sensing of natural emissions (ground or space-based).

(a) Absorption of cosmic radio waves; radio star refraction
(b) Aurora—interferometry and imaging
(c) Natural airglow—temperature and velocity of the emitting gases

These techniques suffer from lack of height discrimination.

In-situ measurements with instruments on rockets and satellites

(a) Density, composition, temperature, velocity of ionized and neutral gas; electric and magnetic fields.
(b) Tracking of objects and chemical trails released from spacecraft (good space and time resolution, no systematic coverage)
(c) Analysis of satellite orbits (air density)

Active experiments

RF heating; releases of active chemicals

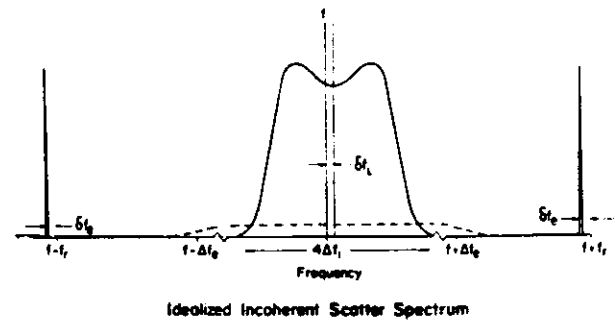

Fig. 4. The incoherent scatter radar spectrum. The width Δf_i and shape of the central 'ion line' depend on the thermal motions of the plasma (and thus on the ion and electron temperatures and the ion composition). Its offset δf_i from the transmitted frequency f is a Doppler shift due to the line-of-sight motion of the ions. The 'plasma lines' flanking the ion line are offset from f by $\pm f_r$ (f_r is approximately equal to the ambient plasma frequency f_0), with a further offset δf_e due to the relative motion of ions and electrons. (From European Space Agency SP-135, p.87, 1978.)

2 The Neutral Atmosphere

2.1 Regions of the Upper Atmosphere

Figure 1 shows the main regions of the neutral atmosphere in relation to the average vertical profile of temperature. They are the troposphere (0–12 km approximately), where the temperature decreases from its ground-level value with increasing height; the stratosphere (12–30 km), a turbulent region of fairly uniform temperature; the mesosphere (30–80 km), a region of higher temperature, heated by the absorption of solar UV radiation by the small amount of ozone; and the thermosphere above 80 km, strongly heated by solar extreme ultraviolet (EUV) and X-rays which dissociate and ionize the atmospheric gases and thus create the ionosphere. In the exosphere above 600 km, the air is too thin to be considered as a gas at all; the individual atoms move freely in satellite-like orbits controlled by the Earth's gravity. Up to about 100 km the major gases, nitrogen (N_2) and oxygen (O_2), are well mixed by winds and turbulence, and their concentration ratio of 4:1 does not change with height. Minor constituents (such as H_2O, CO_2, NO and O_3) are largely controlled by chemical reactions, and their distributions do not necessarily follow the same trend as the major gases.

Above 100 km, two changes occur. First, oxygen (but not nitrogen) largely becomes dissociated into atoms by the action of solar UV radiation. Second, turbulence ceases at the turbopause near 100 km, and the gases are diffusively separated by the action of gravity, so that atomic oxygen (molecular mass $M = 16$) progressively becomes more abundant than molecular nitrogen and oxygen ($M = 28$, 32). This is shown in Fig. 5, which also compares the distributions of the main charged and neutral constituents. Higher still, the lightest gases, hydrogen and helium, become dominant in the exosphere, from which they slowly escape.

2.2 The Hydrostatic Equation and Scale Height

The vertical distribution of any gas is controlled by gravity, which balances the vertical pressure gradient. This balance is expressed by the hydrostatic or barometric equation

$$-\mathrm{d}p/\mathrm{d}h = \rho g = nmg \qquad (5)$$

where p = pressure, ρ = density, n = concentration, m = particle mass and g = acceleration due to gravity. This equation may be combined with the perfect gas law

$$p = nkT = \rho RT/M \qquad (6)$$

where k = Boltzmann's constant, R = gas constant and M = molar mass, and then integrated with height to give the variation of pressure with height above any chosen base level h_0, at which the pressure is p_0:

$$p = p_0\, \mathrm{e}^{-z} \approx p_0 \exp\left[(h_0 - h)/H\right] \qquad (7)$$

where

$$z = \int_{h_0}^{h} (\mathrm{d}h/H) \approx (h - h_0)/H \qquad (8)$$

and

$$H = kT/mg = RT/Mg \qquad (9)$$

H is known as the scale height of the gas and z as the reduced height (measured in units of H); the expressions in (7) and (8) following the symbol $\approx$ hold if H is constant with height. Despite the steep temperature gradient between about 90 and 200 km, the simplified expressions are often useful. It is easily shown that the total number of particles in a vertical column above any height h_0 is $H.n(h_0)$, so H may be regarded as 'the thickness of the atmosphere'. Below 100 km the atmosphere is mixed, and all the major gases have the same scale height, with a mean molar mass of 29. However, in the diffusively separated atmosphere above 100 km, each gas has its own scale height corresponding to its molar mass.

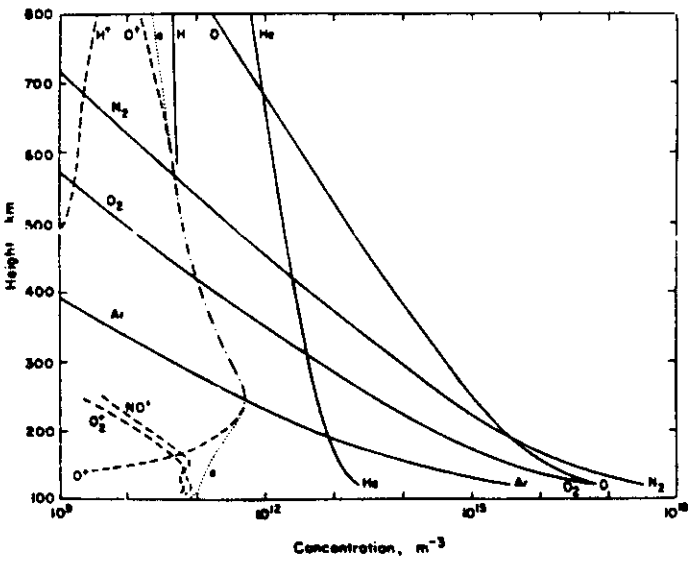

Fig. 5. Neutral and ionized constituents of the upper atmosphere for average daytime conditions at midlatitudes, taken from the COSPAR International Reference Atmosphere, with positive ion distributions by C.Y. Johnson, *J. Geophys. Res.*, **71**, p. 330, 1965. (From *Contemporary Physics*, **14**, p. 231, 1973, Taylor & Francis, London.)

2.3 Upper Atmosphere Temperature

As shown in Fig. 1, the temperature of the thermosphere varies with height. At the base, it is governed by the mesopause temperature (about 180 K), but it increases rapidly upwards with a gradient $\mathrm{d}T/\mathrm{d}h$ determined by the solar heat input. Higher up, the thermal conductivity of the air becomes large and, in consequence, the temperature gradient $\mathrm{d}T/\mathrm{d}h$ flattens out. Above about 300 km, T tends to a limit known as the exospheric temperature T_∞, which varies considerably with local time (LT), latitude, season and the 11-year sunspot cycle. Typically at mid-latitudes T_∞ = 800 K at midday and 600 K at midnight at sunspot minimum, and 1400 K and 1100 K respectively at sunspot maximum. T_∞ is raised locally in the auroral ovals, because of the energy deposited by energetic particles and electric currents from the magnetosphere.

From observations of satellite orbits, which yield extensive data on air density, it has been deduced that T_∞ is highest around 14 LT and lowest around 03 LT; the maxima and minima are in low latitudes near equinox but migrate seasonally. Figures 6 and 7 are maps of T_∞ for March equinox and June solstice, showing some (but by no means all) of the known complexity. The temperature variations are mainly due to solar heating, which causes the atmosphere to expand or bulge on the daylit side of the Earth, creating a high-pressure region often referred to as the daytime pressure bulge. Localized heating in the auroral ovals is not shown in these maps.

The chemical composition also varies with time and season. For example, the O/N_2 ratio above 200 km is greater in winter than in summer, while localized variations of composition occur in auroral latitudes. These variations arise, in a complicated way, from the global thermospheric circulation described in Section 2.4.

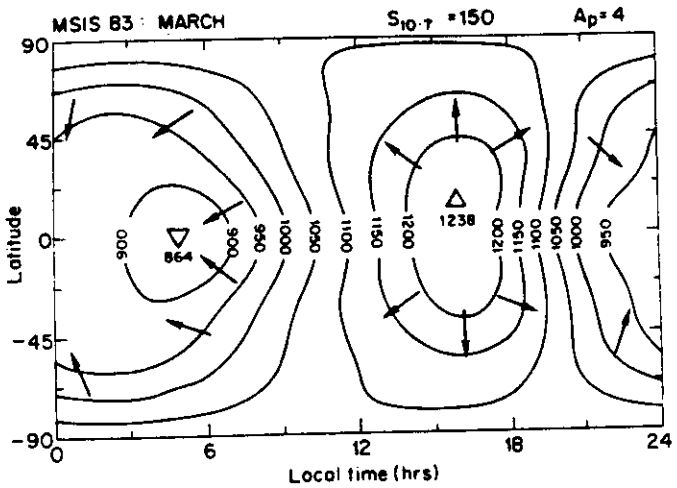

Fig. 6. Map of exospheric temperature at March equinox, for high solar activity and quiet geomagnetic conditions, according to the MSIS83 thermospheric model by A.E. Hedin, *J. Geophys. Res.*, **88**, p. 10170, 1983. Arrows show the approximate directions of the thermospheric winds. (*Courtesy of* S.E.R.C. Rutherford Appleton Laboratory.)

2.4 Upper Atmosphere Winds

The thermosphere is a vast heat engine driven by solar, auroral and interplanetary sources. The energy from these sources produces the temperature variations shown in Figs 6 and 7, giving rise to horizontal pressure gradients and winds. These winds, together with the associated vertical upcurrents and downcurrents, form a global circulation that carries energy away from the heat sources and liberates it elsewhere.

The neutral-air wind velocity **U** is controlled by the Coriolis force due to the Earth's rotation with angular velocity Ω; the molecular viscosity of the air (coefficient μ); and ion-drag, which is due to collisions between air molecules and ions, and exists because the ions are constrained by the geomagnetic field and cannot move freely with the wind. This frictional force depends on the ion-neutral collision frequency and on the difference between the wind velocity **U** and the ion velocity **V**, which is mainly due to electromagnetic forces (Section 4.4). The equation of motion for the horizontal wind is then

$$d\mathbf{U}/dt = \mathbf{F} - 2\Omega \times \mathbf{U} - KN(\mathbf{U} - \mathbf{V}) + (\mu/\rho)\nabla^2 \mathbf{U} \quad (10)$$

where

$$\mathbf{F} = -(1/\rho)(\partial/\partial x, \partial/\partial y)\, p \quad (11)$$

is the driving force due to the horizontal pressure gradient, and K is the 'ion-neutral collision coefficient'. At great heights (small ρ) the ratio (μ/ρ) becomes very large, so that $\nabla^2 \mathbf{U}$ has to become small, i.e. viscosity tends to destroy spatial variations of **U**. As a result, $d\mathbf{U}/dh \to 0$ and the wind varies little with height. Lower down, (μ/ρ) is smaller and small-scale velocity gradients are not smoothed out by viscosity.

The wind direction depends on the ratio of Coriolis force to ion-drag. This may be illustrated by considering some special steady-state cases of equation (10) in which $d\mathbf{U}/dt = 0$ and viscosity is neglected. If the Coriolis force is dominant and ion-drag is small, as in the lower ionosphere, the wind blows at right angles to the pressure gradient. Then, at latitude ϕ,

$$U = F/(2\Omega \sin\phi) \qquad (\mathbf{U} \perp \mathbf{F}) \quad (12)$$

This is the situation familiar in weather maps for the lower atmosphere, with the wind blowing along the isobars of constant pressure. A very different situation exists in the daytime F layer, where ion-drag is large and the wind is almost parallel to the pressure-gradient force, so that

$$U = F/(KN \sin I) \qquad (\mathbf{U} \parallel \mathbf{F}) \quad (13)$$

where I is the magnetic dip angle. In the intermediate case, both ion-drag and Coriolis force are significant and the wind is inclined to **F** at the angle

$$\psi = \arctan\left(\frac{2\Omega}{KN}\sin\phi\right) \quad (14)$$

and its magnitude is approximately given (except in equatorial latitudes) by

$$U = \frac{F}{\sqrt{(K^2N^2\sin^2 I + 4\Omega^2\sin^2\phi)}} \quad (15)$$

Accordingly, the schematic wind vectors shown in Figs 6 and 7 are nearly parallel to the temperature (and pressure) gradient by day, but are slightly deflected by Coriolis force at night.

If the ions are drifting under the influence of an electric field, they set the air into horizontal motion, i.e. the ion-drag term in equation (10) acts as a driving force. The wind direction is then determined by the ratio of Coriolis force to ion-drag, just as in equation (14). In high latitudes, these 'electrically-driven' winds may predominate, though auroral heating produces localized pressure gradients and associated thermal winds, so both pressure gradient and ion-drag terms must be considered. At lower latitudes, thermal winds driven by solar heating dominate, though electric fields are important in the vicinity of the magnetic equator.

The neutral air velocity is of course subject to equations of continuity and energy, as well as to the equation of motion (10). Production and loss processes are unimportant for the major constituents of the neutral air, and the continuity equation (1) reduces to

$$\partial n/\partial t = -\operatorname{div}(n\mathbf{U}) \quad (16)$$

The pressure distribution and the wind velocity automatically adjust themselves to satisfy equation (16). Thus any divergence (or convergence) of the horizontal winds must be balanced by upward (or downward) winds, so that

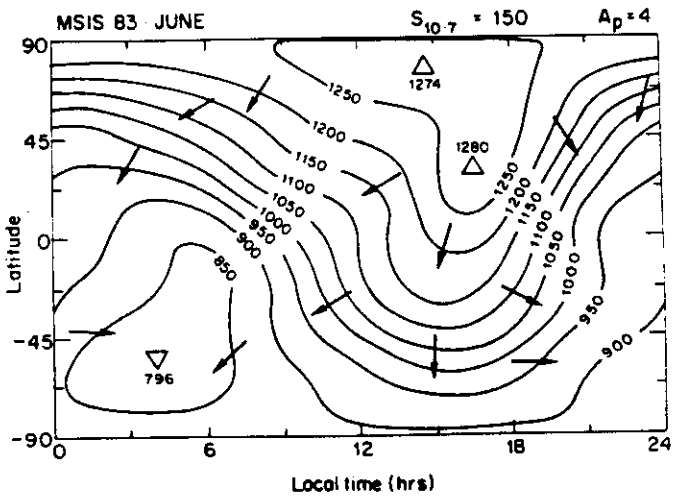

Fig. 7. As Fig. 6, for June solstice (*Courtesy of* S.E.R.C. Rutherford Appleton Laboratory.)

in the lower atmosphere) are nearly divergence-free, and are ineffective in removing the horizontal pressure differences that drive them.

2.5 Atmosphere Tides[6]

The thermospheric winds just described are part of a complex system of atmospheric tides, which can be resolved into numerous components. Tides are 'forced' or driven by the heating effect of the Sun, or by the gravitational attraction of the Sun and Moon. The solar thermal tide, which predominates in the upper atmosphere (unlike the case of marine tides, in which the lunar gravitational tide predominates) is driven by:

(a) absorption of solar EUV and X-rays in the thermosphere;
(b) absorption of solar UV in the ozone layer;
(c) heating of the ground and lower atmosphere by visible and infra-red radiation.

The heating sets up tidal modes denoted by index numbers (n,m), in which $n = 1$ for 24-hour diurnal modes, $n = 2$ for 12-hour semidiurnal modes etc., and m is a positive or negative integer that defines the latitude structure of the mode. As well as the solar diurnal tide, a few semidiurnal modes are also important in the thermosphere. Gravitational forcing has a fundamental semidiurnal period, 12 hours for solar tides and 12·4 hours for lunar tides. These wind systems produce geomagnetic variations through the dynamo effect (Section 4.5).

2.6 Gravity Waves[7]

The atmosphere contains many kinds of waves, ranging in period from the 26-month quasi-biennial oscillation to infrasonic waves of periods < 1s, some of which are associated with aurora or seismic activity. They include planetary waves with wavelengths of the order of 1000 km and periods of days, tidal waves as described in Section 2.5, and acoustic and gravity waves.

These waves represent solutions of wave dispersion equations which are derived from the appropriate form of equations (1)–(3). Acoustic waves are oscillations of period < 4 min, in which the restoring force is provided by compression and gravity is unimportant. Gravity waves are oscillations controlled by the buoyancy of the air, i.e. by gravity, and have a minimum period of about 5 min (the Brunt-Väisälä period) in the thermosphere. Unlike ocean waves, which are virtually confined to the surface, gravity waves permeate the whole upper atmosphere. They can be divided into two classes, as follows:

(a) Short-period and medium-period gravity waves (periods of 5–30 min, wavelengths of 100–300 km, horizontal speeds of 100–200 m s^{-1}) are generated in the lower atmosphere by storms, by winds blowing over mountains, and occasionally by man-made explosions.
(b) Long-period gravity waves (periods of 0·5–3 hours, horizontal wavelengths of 1000–4000 km, speeds of 400–700 m s^{-1}) are generated by disturbances in the thermosphere, mainly in the auroral oval. They can travel for thousands of kilometres and are prevalent at times of geomagnetic disturbance.

Gravity waves have a complicated phase structure. In addition to the horizontal propagation, the phase velocity has a downward component which gives the appearance of a downward travelling wave, although the group velocity and energy propagation is in fact inclined slightly upwards. The amplitude and phase of the oscillations of air pressure, density and temperature, and of the oscillatory air velocity within the wave, are wavelike functions of time t and position $\mathbf{r}$. Thus, for a wave of angular frequency w and wavenumber $\mathbf{k}$ the pressure oscillation is of the form

$$\Delta p/p \propto e^{z/2} \exp i(wt - \mathbf{k}.\mathbf{r}) \qquad (17)$$

and similarly for the other parameters. As shown by the exponential factor $e^{z/2}$, the wave amplitude increases upwards such that the kinetic energy density $\frac{1}{2}\rho u^2$ is independent of height (since the air density ρ decreases upwards, roughly as e^{-z}). This increase is limited in three ways:

(i) by partial or total reflection, depending on the thermal structure of the atmosphere (because, as can be shown from the dispersion equation, it tends to occur at levels where $dT/dh > 0$); it causes the waves propagated up from the lower atmosphere to be selectively filtered, in a manner that varies with season;
(ii) by dissipation, by ion-drag or viscosity;
(iii) if the amplitude $\Delta p/p$ becomes so large that the wave breaks, i.e. it becomes non-linear and the wave is degraded into smaller-scale motions. Some solar tidal modes may become large enough to undergo non-linear interaction, but usually dissipation or reflection takes place before that occurs.

3 The Ionospheric Layers

3.1 Ionizing Solar Radiations

The principal ionospheric layers are produced by extreme ultraviolet (EUV) and X-rays, emitted from the Sun as spectral lines and continuum radiation. The level in the atmosphere to which any wavelength λ penetrates depends on its absorption cross-section σ (or its 'hardness'), and the gases it can ionize are those for which λ is shorter than the ionization limit (80 nm for N_2, 91 nm for O and H, 103 nm for O_2 and 134 nm for NO). The principal radiations that produce the ionospheric layers are (Fig. 2):[8]

F1 layer (150–180 km): EUV 17–80 nm (the softest EM radiation)
E layer (100–120 km): X 1–17 nm, and EUV 91–103 nm (Ly β 102·6 nm)
D layer (70–90 km): Ly α 121·6 nm (NO) and X-rays 0·1–1 nm, etc
C layer (50–70 km): MeV cosmic rays (not a significant layer)

The heights shown are those where the radiations are most strongly absorbed (Section 3.2). There is *no* ionizing photon radiation that is strongly absorbed above the F1 layer, so the F1 and F2 layers must be formed by the same radiation, and the greater electron density of the F2 layer is due to a smaller rate of loss of electrons (Section 4.2). Charged particles can also ionize the air, and the height to which they penetrate depends on their energy or hardness; such ionization is important in high latitudes, particularly in the auroral ovals.

3.2 Chapman Layers

The simple Chapman theory of the production of an ionized layer starts by assuming (a) monochromatic solar radiation acting on (b) a plane atmosphere containing (c) a single ionizable gas with (d) a constant scale height. All four simplifications (a–d) can be removed, but the equations become more complicated.

Radiation, initially of intensity I_∞, strikes the top of the atmosphere at zenith angle (obliquity) χ, and its intensity $I(h)$ decreases as it travels downards, according to the equation

$$(dI/I) = -\sigma n\, dh \sec \chi = -d\tau \qquad (18)$$

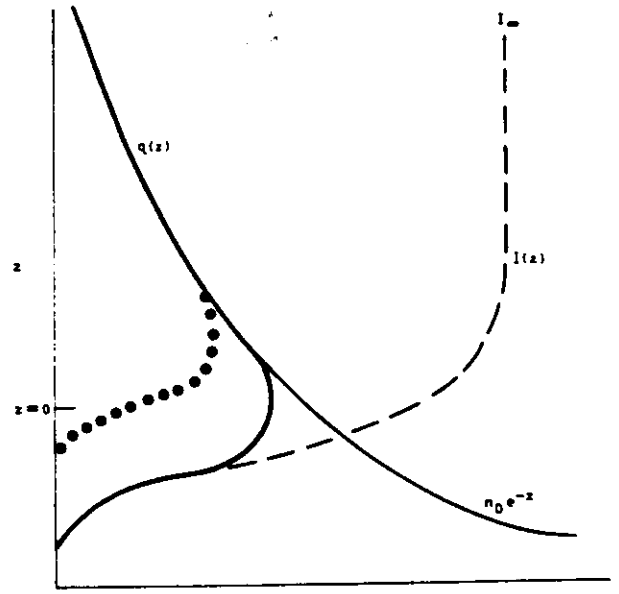

Fig. 8. Theoretical curves of ion production, illustrating equations (19) and (20). For overhead sun, the downcoming radiation, of initial intensity I_∞, is attenuated as shown by the dashed curve $I(z)$, by absorption in the gas which is distributed according to the exponential curve $n_0 e^{-z}$. The production function $q(z)$ is then proportional to the product of $I(z)$ and $n_0 e^{-z}$. For oblique sun, attenuation begins at a greater height, and the production function $q(z)$ is modified as shown by dots. (*Courtesy of* S.E.R.C. Rutherford Appleton Laboratory.)

where σ is the absorption cross-section and τ is optical depth. By integrating equation (18) along the path of the radiation, from the top of the atmosphere down to height h, and using the property that $\int n\, dh = n(h).H$ (Section 2.2), it is found that

$$I(h) = I_\infty \exp(-n\sigma H \sec\chi) = I_\infty e^{-\tau(h)} \qquad (19)$$

The production rate q (see Fig. 8) is found by multiplying the intensity of the radiation (dashed curve) by the gas concentration n (continuous curve), and also by the cross-section σ and ionizing efficiency η. Thus

$$q(h) = I(h)\,\eta\sigma\, n(h) = I_\infty\,\eta\sigma\, n(h)\, e^{-\tau(h)} \qquad (20)$$

On differentiating equation (20), it is found that the peak value of q occurs at the height where $\tau = 1$ (unit optical depth), and is given by

$$q_0 = (\eta I_\infty / eH)\cos\chi \quad \text{at} \quad z = \ln\sec\chi \qquad (21)$$

Using the reduced height z, q is given by the Chapman formula

$$q(z,\chi) = q_0 \exp(1 - z - e^{-z}\sec\chi) \qquad (22)$$

3.3 Critical Frequency

The 'ordinary mode' critical frequency f_0 of an ionospheric layer is related to its peak electron density N_m by

$$f_0^2 = 80{\cdot}6\, N_m \quad \text{or} \quad f_0 \approx 9\sqrt{N_m} \qquad (23)$$

where the numerical factors (MKS) are derived from physical constants. (f_0 is the plasma frequency of Section 1.4; there is also a slightly higher extraordinary mode critical frequency f_x, because of the double refraction of radio waves caused by the Earth's magnetic field). For a simple Chapman layer in which electrons are produced according to equation (22) and recombine according to a square law αN^2 (Section 4.1), the critical frequency depends on solar zenith angle χ and the mean sunspot number R, according to the formula

$$f_0 = A(1 + aR)(\cos\chi)^n,\ n = 0{\cdot}25 \qquad (24)$$

where A and a are constants. The daytime E and F1 layers follow this formula quite well when χ varies with time of day, season, and latitude. Because of complications (e.g. the variation of scale height H with height, and the effect of vertical drifts) the index n actually varies between about 0·2 and 0·35. The incident solar flux I_∞ varies with the solar cycle, and so f_0 varies regularly with the sunspot number. Figure 9 shows the regular seasonal and solar cycle variations of the E and F1 layers. The normal D layer (though not possessing a measurable critical frequency) also varies quite regularly with cos χ. The F2 layer does not; careful examination of the seasonal ripple

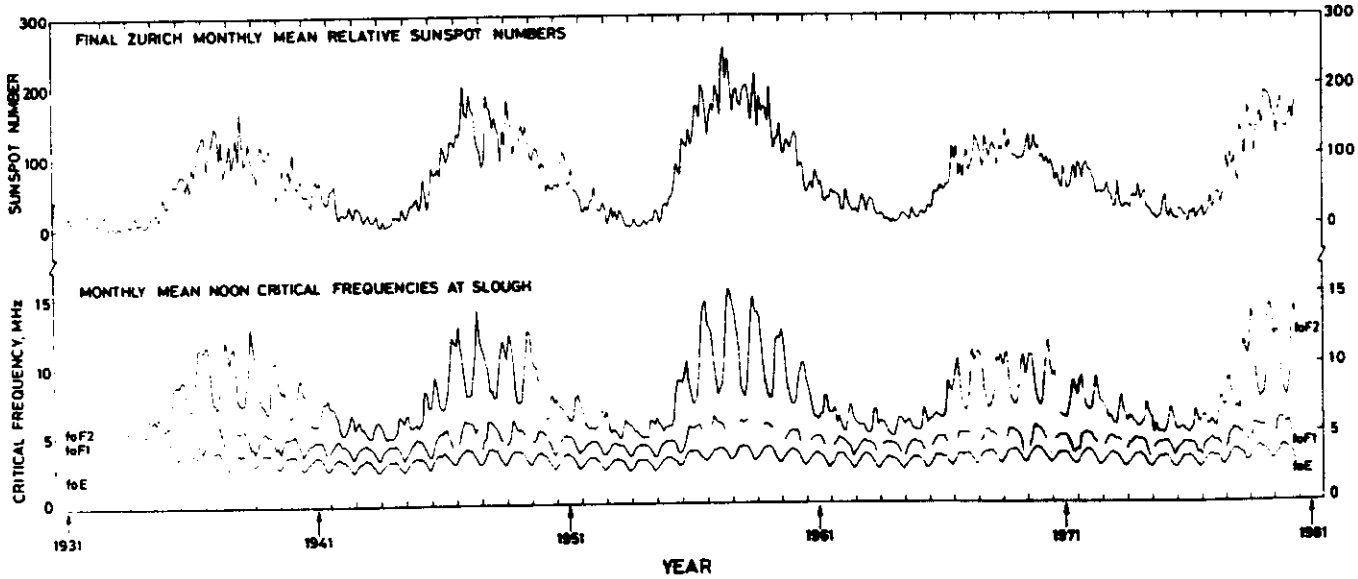

Fig. 9. Noon monthly mean critical frequencies of the F2, F1 and E layers at Slough (Lat. 52°N, 1931–1981). (*Courtesy of* S.E.R.C. Rutherford Appleton Laboratory.)

of foF2 shows that it is out of phase with those of the F1 and E layers, which do conform to the variation of $\cos \chi$.

4 Basic Ionospheric Processes

4.1 The Continuity Equation

The continuity equation (1) for electrons and ions is

$$\partial N/\partial t = q - L(N) - \text{div}\,(N\mathbf{V}) \qquad (25)$$

The loss term $L(N)$ can generally be simplified as follows:

$$\text{E layer: } L(N) = \alpha N^2 \quad \text{F2 layer: } L(N) = \beta N \qquad (26)$$

where α, β are the square-law and linear loss coefficients. The transport term can generally be simplified by omitting horizontal motion, which contributes little to equation (25), and including only the vertical drift velocity W, in which case

$$\text{div}\,(N\mathbf{V}) = \partial(NW)/\partial h \qquad (27)$$

4.2 Ion Chemistry and Loss Processes

The ion composition shown in Fig. 5 results from a variety of photochemical processes. To understand how these processes affect the ionosphere, and why they result in the types of loss term given by equation (26), some basic ideas are needed. Numerical values of the coefficients may be found in the literature, e.g. in Reference 9.

Reactions in the ionosphere have to conserve energy and momentum (besides satisfying the principles of quantum theory). One consequence is that atomic ions cannot recombine easily with electrons, unless a third body takes part in the reaction and absorbs the excess energy. This requires a 3-body collision, which is only likely to occur below 100 km, where the air density is sufficiently high. Molecular ions, however, recombine easily at any height, since they can dissociate to give two products. Throughout the ionosphere, reactions may leave atoms and molecules in excited states, which subsequently decay by emitting radiation. This is the origin of the upper atmosphere luminescence, the airglow. To summarize for the main layers:

D layer: The atmosphere is relatively dense, so both 2-body and 3-body collisions occur and complicated chemical reactions take place. Electrons may become attached to atoms and molecules, to form negative ions. Negative ions are more abundant than electrons at all heights below 90 km at night but, being destroyed by visible and ultraviolet sunlight, they are only abundant below 70 km by day. Many ions, both positive and negative, become attached to water molecules to form complex clusters.

E layer: The atmosphere is more rarified and only 2-body collisions occur, so atomic ions cannot recombine easily with electrons; molecular ions recombine easily. The overall result is that the positive ions are mostly molecular, NO^+ and O_2^+; and the loss coefficient α is of the square-law type in equation (25). Some metal atoms (Fe, Mg, Ca), traces of which are deposited in the atmosphere by meteors, become charged, giving long-lived ions that are the main ionic component of mid-latitude sporadic E layers.

F layer: The ions are predominantly NO^+ and O_2^+ in the E and F1 layers, but O^+ in the F2 layer (Fig. 5). The relatively simple chemistry may be summarized as follows:

Production: The major gases are ionized by EUV photons ($h\nu$) of the radiations mentioned in Section 3.1, giving O^+, N_2^+ and some O_2^+ ions, plus electrons. For example:

$$O + h\nu \rightarrow O^+ + e^- \qquad (28)$$

$$N_2 + h\nu \rightarrow N_2^+ + e^- \qquad (29)$$

Charge Transfer: Ions collide with neutral molecules and undergo certain transfer reactions, of which these are the most important:

$$O^+ + O_2 \rightarrow O_2^+ + O \qquad (30)$$

$$O^+ + N_2 \rightarrow NO^+ + N \qquad (31)$$

$$N_2^+ + O \rightarrow NO^+ + N \qquad (32)$$

Recombination: The ions recombine with electrons and dissociate:

$$NO^+ + e^- \rightarrow N + O \qquad (33)$$

$$O_2^+ + e^- \rightarrow O + O \qquad (34)$$

$$N_2^+ + e^- \rightarrow N + N \qquad (35)$$

The atoms produced in these recombination reactions are generally in excited states. The excess energy is either lost in collisions, or is radiated as ultraviolet, visible or infrared airglow.

This scheme accounts for otherwise puzzling facts:

(i) Despite the abundance of neutral N_2 there are very few N_2^+ ions; they are rapidly destroyed by reaction (32) as well as (35).
(ii) NO^+ ions are very abundant although neutral NO is very scarce, NO^+ being rapidly formed by reactions (31) and (32).
(iii) Below about 200 km, molecular ions dominate; this is because the O^+ ions are rapidly converted to NO^+ and O_2^+ by the relatively abundant N_2 and O_2.
(iv) Above about 200 km, the relative scarcity of N_2

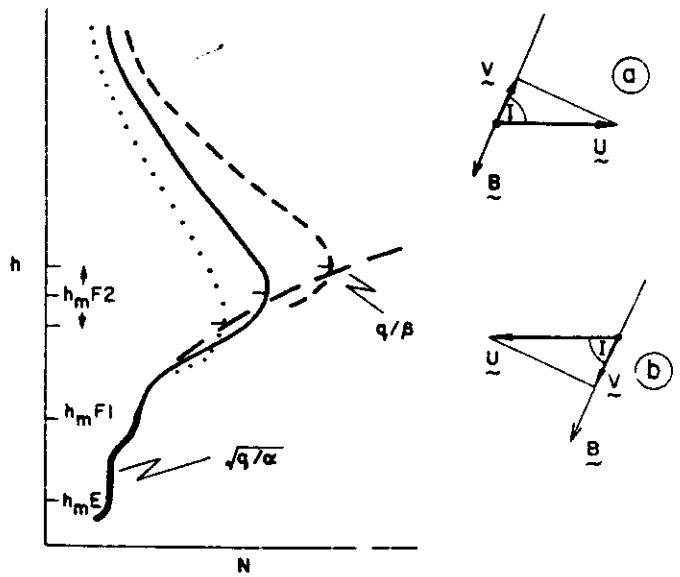

Fig. 10. Idealized electron density profiles in the E and F1 layers, with square-law loss coefficient; and in the F2 layer, with linear loss coefficient. The effects of upward and downward drift on the F2 peak are shown by dashed and dotted curves, respectively. The sketches on the right show the ion drift V produced by a horizontal wind U in the neutral air, the vector B representing the geomagnetic field (dip angle I). (a) Upward field-aligned drift is produced by a wind blowing towards the magnetic equator; (b) downward drift is produced by a wind blowing towards the magnetic pole. (From *Contemporary Physics*, 14, p. 244, 1973, Taylor & Francis, London.)

and O_2 makes reactions (30) and (31) very slow. Once formed, however, the NO^+ and O_2^+ ions rapidly recombine with electrons by reactions (33), (34). As a result, O^+ is the dominant ion.

Further analysis shows that this scheme has other consequences:

(v) The loss term takes the form αN^2 at heights where NO^+ and O_2^+ ions dominate, i.e. the E and F1 layers, as in equation (26).
(vi) The loss term takes the form βN where O^+ dominates (F2 layer).
(vii) The F1 layer, at the transition between (v) and (vi), is seen as a distinct feature with its own critical frequency under certain circumstances (mainly summer and at sunspot minimum) but not at other times (e.g. winter); see Section 5.4.
(viii) Above the F1 layer, the electron density increases upwards; this is because the loss coefficient β (which depends on the N_2 and O_2 concentration) decreases upwards faster than the production rate q (proportional to O concentration).

Figure 10 shows the general form of the $N(h)$ profiles that result from these processes. Whether or not the F1 layer appears as a distinct layer depends on the ratio G (evaluated at F1 peak), defined by

$$G = \beta^2/\alpha q \tag{36}$$

where the coefficients α, β are as defined in equations (26). For the E and F1 layers, the effective square-law loss coefficient is a combination of the values of α for the molecular ions present. For the F2 layer, the linear loss coefficient is

$$\beta = K'n[O_2] + K'' n[N_2] \tag{37}$$

where K', K'' are the rate coefficients of reactions (30), (31).

4.3 Equation of Motion of the Charged Particles

The simplified equations of motion for singly charged positive ions, and for electrons, are

$$m_i\, d\mathbf{V}_i/dt = m_i \mathbf{g} + e\mathbf{E} + e\mathbf{V}_i \times \mathbf{B} + m_i\nu_i(\mathbf{U}-\mathbf{V}_i) - \nabla p_i/N \approx 0 \tag{38}$$

$$m_e\, d\mathbf{V}_e/dt = m_e\mathbf{g} - e\mathbf{E} - e\mathbf{V}_e \times \mathbf{B} + m_e\nu_e(\mathbf{U}-\mathbf{V}_e) - \nabla p_e/N \approx 0 \tag{39}$$

The acceleration terms ($d\mathbf{V}_i/dt$, $d\mathbf{V}_e/dt$) are negligible for the large-scale motions considered here, so the sum of the forces acting on the particles can be set equal to zero. The relevant forces are due to gravity **g**, the electrostatic field **E**, the geomagnetic field **B**, frictional drag by the neutral air, and the gradient of the ions' or electrons' own partial pressure p_i, p_e. The symbol e denotes the elementary positive charge (so that $-e$ is the charge on an electron), ν the collision frequency between charged particles and neutral particles, and identifying suffixes 'i' and 'e' are added as necessary.

4.4 Motion produced by Winds and Electric Fields

Only a few special cases of equations (38) and (39), relevant to the flow of electric currents in the E layer (Sections 4.5, 4.6) and the behaviour of the F2 layer (Section 4.7), need to be discussed here. A single kind of positive ion is assumed, and negative ions are ignored (though the equations could be generalized, if necessary, to include negative ions, or multiple species of positive ion). Deleting the acceleration, gravitational and pressure gradient terms in equations (38) and (39), these equations can be solved to give the following results:

For motion $\parallel$ **B**: if the neutral air wind has a component $U_\parallel$ along **B**, both ions and electrons move freely along **B** with that speed. If the electric field has a component $E_\parallel$ in that direction, electrons and ions flow freely in opposite directions, thus creating a high conductivity as discussed in Section 4.5.

For motion $\perp$ **B**: the direction of motion depends on the ratio of the collision frequency ν (with neutral particles) to the magnetic gyrofrequency $\omega = Be/m$. Since ν decreases exponentially upwards, while ω is almost constant, the ratio ν/ω falls off rapidly with height; it is different for ions and electrons. Figure 11 illustrates the most important cases:

(i) $\nu \gg \omega$ (up to 100 km for ions, 60 km for electrons). A wind drives the ions and electrons at its own speed, and the magnetic field has no effect. An electric field moves ions parallel and electrons antiparallel to itself, but only slowly because of the high collision frequency, so the conductivity is low.
(ii) $\nu \approx \omega$ (at about 125 km for ions, 75 km for electrons). A wind or an electric field drives ions and electrons in directions inclined to the applied force, as sketched in Fig. 11. The angle is given by arc tan (ω/ν), and is thus 45° at the level where $\nu = \omega$.
(iii) $\nu \ll \omega$ (above 150 km for ions, 90 km for electrons). The particles move at 90° to the applied force. An electric field moves both ions and electrons at speed E/B in the same direction; this is the electromagnetic drift velocity or Hall drift, written vectorially as $\mathbf{E} \times \mathbf{B}/B^2$. Since electrons and ions move at almost exactly the same velocity, there is virtually no current. A neutral air wind **U** produces practically no motion of ions and electrons across the magnetic field.

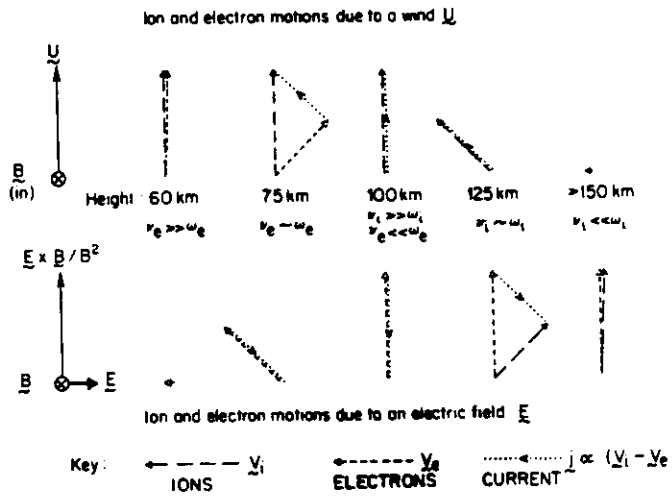

Fig. 11. Ion and electron motions produced by a wind **U** or an electric field **E**, perpendicular to the geomagnetic field vector **B** (directed into page), at five different heights. The current is proportional to $\mathbf{V}_i - \mathbf{V}_e$. Note that (as shown by the small arrows) at 60 km an electric field has only a very small effect on the electrons, and no effect on the ions; above 150km a wind has no effect on the electrons, and little effect on the ions. (*Courtesy of* S.E.R.C. Rutherford Appleton Laboratory.)

If the positive ions and electrons move at different velocities (as happens at heights where the ratio ν/ω is different for ions and electrons) an electric current flows, of density

$$\mathbf{j} = Ne(\mathbf{V}_i - \mathbf{V}_e) \tag{40}$$

Most texts on the ionosphere discuss the relation between electric field **E** and current density **j** in terms of the electrical conductivity σ, which is a tensor quantity because **j** and **E** are usually not parallel. This is really a different way of expressing the physics discussed in Section 4.4. The components of this tensor can be derived from equations (36) and (37) and are as follows:

Longitudinal conductivity, σ_0, the ratio of the electric current and electric field components parallel to the geomagnetic field. This current is carried almost entirely by the electrons, as they are more mobile than the ions.
Pedersen conductivity, σ_1 or σ_P, which relates the electric field $E_\perp$ (normal to **B**) to the current in that direction. This current is carried by the ions, and peaks at around 125 km (where $\omega = \nu$ for the ions). Some Pedersen current flows in the F layer.
Hall conductivity, σ_2 or σ_H, which relates to the current in the direction normal to both **E** and **B**. The Hall current, carried by electrons, is the main part of the total ionospheric current.

Combining the conductivities gives a general relation between electric field and current density (Ohm's Law for the ionosphere):

$$\mathbf{j} = \sigma_0 \mathbf{E}_\parallel + \sigma_1 \mathbf{E}_\perp + \sigma_2 (\mathbf{B} \times \mathbf{E}_\perp)/B \tag{41}$$

Since the ionosphere is always very nearly electrically neutral, the current cannot produce any appreciable density of electric charge, but must be non-divergent:

$$\operatorname{div} \mathbf{j} = 0 \tag{42}$$

As mentioned in Section 4.4, electrons and ions flow freely along the geomagnetic field lines. The high longitudinal conductivity σ_0 effectively creates a short circuit along any geomagnetic field line, throughout the ionosphere and magnetosphere. This has several consequences. First, the short-circuiting effect means that no significant *steady* field $\mathbf{E}_\parallel$ can be maintained parallel to the geomagnetic field. Second, electric currents can flow freely between opposite hemispheres, to keep magnetically conjugate points in the ionosphere at (very nearly) the same electric potential, i.e. the geomagnetic field lines are electric equipotentials. Third, the electric field perpendicular to **B** is almost independent of height within the ionosphere, which implies that the electric fields generated in the E layer also permeate the overlying F layer and magnetosphere. As a result, the drift velocity ($\mathbf{E} \times \mathbf{B}/B^2$) in the F layer and magnetosphere is closely related to that in the underlying E layer.

4.6 Dynamo Theory

At mid-latitudes, the electric current in the ionosphere is mostly produced by the atmospheric dynamo in the E layer, driven by the tidal winds described in Section 2.5. At this height, $\nu \gg \omega$ for ions but $\nu \ll \omega$ for electrons (Section 4.4). The winds accordingly move the ions across the geomagnetic lines of force, but cannot drive the electrons. As the ions and electrons move differently, a current flows—as given by equation (40)—and charge separation takes place, building up an electric polarization field which modifies the ion and electron motions. Very quickly, the motions, the current, and the polarization field adjust themselves in such a way that no further charge separation occurs; the situation is then stable, but constantly re-adjusts itself as the winds change. Very little current flows at heights below 100 km because the electron density N is so small (Fig. 2); the bulk of the current flows between 100 km and 125 km (the level at which $\nu = \omega$ for the ions). At night, N is small even at 100–125 km, so the current is weak.

An alternative treatment of dynamo theory, found in most textbooks, describes the process of current generation as follows: the tidal wind **U** drives the ionization across the geomagnetic field, creating an induced electric field $\mathbf{U} \times \mathbf{B}$. Since the resulting current does not, in general, satisfy the condition (42), it causes a very small accumulation of electric charge, producing an electrostatic field which adjusts itself so that the total electric current is divergence-free. This alternative description is equivalent to that given above.

At the magnetic dip equator, owing to the special geometry, a strong vertical polarization field develops in the E layer (as may be shown by a detailed study of the equations of motion). This field has the effect of creating a very high electric conductivity in the east-west direction, almost as large as the longitudinal conductivity σ_0. In consequence, a strong east-west current, called the equatorial electrojet, flows in a narrow belt covering about 3° either side of the dip equator (Section 5.6).

Besides the wind-driven dynamo fields and currents, electric fields and currents are generated in the magnetosphere and transmitted along geomagnetic field lines to the high latitude ionosphere, and spread to some extent to lower latitudes. They are responsible for the large-scale convection described in Section 5.9. Strong localized east-west currents, the auroral electrojets, flow in the auroral ovals, especially during magnetic storms. They are driven by strong electric fields generated in the magnetosphere, and are a major source of high-latitude heating (Section 2.3).

4.7 The F2 Peak

Section 4.2 (viii) explained why the electron density increases upwards from the F1 layer, according to the ratio q/β. The increase stops when gravity eventually controls the ion distribution. The F2 peak thus occurs at the height where chemical control gives way to gravitational or diffusive control. At the F2 peak, the transport terms in the continuity equation (25) are comparable to production and loss, which are roughly in balance below that height. The $N(h)$ profile then looks roughly as in Fig. 10. Introducing the diffusion coefficient D for the ions, which is inversely proportional to the ion-neutral collision frequency ν_i, the F2 peak is governed by the following relations (in which the suffix 'm' denotes values at the peak height h_mF2, and using equations (20) and (37)):

$$\beta_m \approx D_m/H^2 \tag{43}$$

$$N_m \approx q_m/\beta_m \propto \frac{I_\infty n[\mathrm{O}]}{K' n[\mathrm{O}_2] + K'' n[\mathrm{N}_2]} \tag{44}$$

Thus N_m depends on the atomic/molecular ratio of the neutral air. As defined by equation (43), the height h_mF2 tends to lie at a fixed pressure-level in the atmosphere, i.e. a fixed value of the reduced height z defined by equation (8).[10]

The height of the peak can be shifted by a neutral air wind or an electric field. A horizontal wind blowing towards the magnetic equator drives the ionization up magnetic field lines, raising the peak and increasing N_m. Opposite effects are produced by a poleward wind (Fig. 10). Poleward winds tend to occur at night (at any rate for the equinox

situation of Fig. 6), equatorward winds by day. Eastward/westward electric fields produce upward/downward electromagnetic drift, i.e. the vertical component of the drift velocity $\mathbf{E} \times \mathbf{B}/B^2$ (Section 4.4), though the effect of this drift on the mid-latitude F2 layer is greatly reduced by the reaction of the neutral air (the 'ion-drag effect').[11]

4.8 The Topside Ionosphere and Ionosphere-Magnetosphere Flow

At heights well above the F2 peak, the ion and electron distribution is diffusively controlled, gravity being balanced by the pressure gradient term in equation (37), much as happens for the neutral air, cf. equation (5) in Section 2.2. Electrostatic forces ensure that the electrons and the ions take up the same scale height (which can be shown to be twice that of the neutral air). Above about 700 km there is a gradual transition from the O^+ ions of the F2 layer to the H^+ ions of the protonosphere; some He^+ ions are also present.

An important feature of the topside F2 layer is the flux of ions and electrons, flowing along the geomagnetic field lines to or from the overlying protonosphere. By day the F2 layer supplies ions to the protonosphere, through the charge-exchange reaction

$$O^+ + H \rightleftharpoons H^+ + O \qquad (45)$$

At night the reverse charge-exchange reaction, accompanied by downward flow, plays an important part in maintaining the O^+ content of the mid-latitude F2 layer, so the protonosphere acts as a reservoir. At higher latitudes, where the geomagnetic field lines are not closed, the ionosphere (particularly at auroral latitudes) acts as a source of energetic O^+ ions to the magnetosphere.[12]

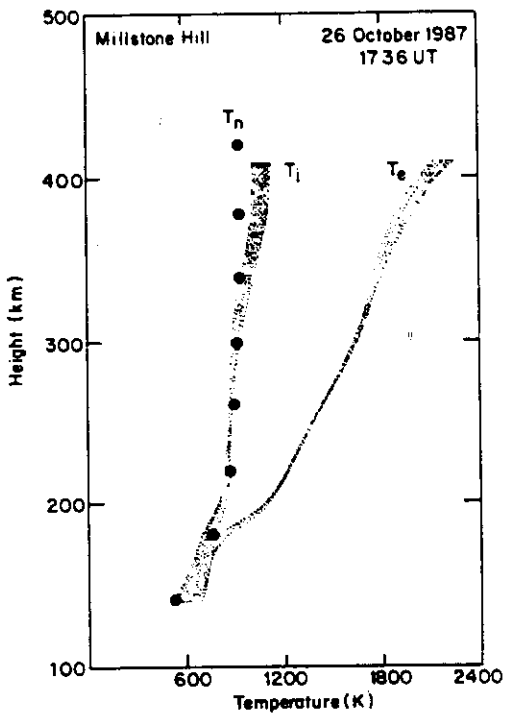

Fig. 12. Ion and electron temperatures as a function of height measured by the incoherent scatter radar at Millstone Hill, USA, (Lat. 43°N) at 1236 LT on 26th October 1987, and analysed by the OASIS program. (*Courtesy of* M.I.T. Atmospheric Sciences Group.) The dots show neutral gas temperatures, according to the MSIS83 thermospheric model of A.E. Hedin, *J. Geophys. Res.*, **88**, p. 10170, 1983.

4.9 Ionospheric Temperatures

It is well established that, in the daytime ionosphere above about 120 km, the electron temperature T_e and ion temperature T_i may exceed the neutral gas temperature T (Fig. 12). The electrons are heated by the 'hot' photoelectrons produced in the ionization reactions (28,29); but loss of heat by collisions with neutral particles or with ions is inefficient because of the great disparity of mass. In consequence, the electron temperature is elevated. The ions, on the other hand, are in good thermal contact with the neutral gas, so that T_i is usually not much different from T at mid-latitudes. However, the large electric fields that occur at high latitudes produce rapid $\mathbf{E} \times \mathbf{B}/B^2$ drifts of the ions (and electrons); collisions between the fast-moving ions and the neutral gas cause 'frictional heating' of the ions (the neutral air is hardly heated at all, because of its much greater thermal capacity). At high latitudes, bombardment by energetic particles can enhance T_e, and very strong heating produces departures from the normal 'Maxwellian' conditions of thermal equilibrium, in the ions as well as the electron gas. A variety of interesting plasma phenomena may then occur.

5 Ionospheric Phenomena

5.1 The D Layer

This paper does not attempt to survey the very complex chemistry of the lower ionosphere, and only a few salient points will be mentioned. From the radio propagation point of view, the D layer plays an important part in LF/VLF propagation; at MF and HF it is important because of its absorbing properties (which stem from the relatively high air density and consequent large collision frequency between electrons and neutral molecules). Increases of D layer electron density therefore affect radio propagation.

During the day, absorption measurements show a fairly regular dependence of D layer ionization on $\cos \chi$. The attachment of electrons to form negative ions at sunset (Section 4.2), and their detachment at sunrise, cause marked changes of LF/VLF reflection height. On some winter days the electron density is abnormally high, apparently because of enhanced concentrations of nitric oxide (which is ionized by solar Lyman α, Section 3.1). These may be connected with dynamical phenomena such as planetary waves.

Some D layer processes are linked with meteorological phenomena at lower heights. For example, the temperature increases (stratospheric warmings) that occur in winter at moderately high latitudes, and represent major changes in the large-scale circulation, are accompanied by increases of radio-wave absorption in the D layer.[13] At auroral latitudes, the D layer is often enhanced by particle precipitation (Section 5.7).

5.2 The E Layer

The normal E layer shows slight departures from idealized Chapman layer behaviour (Section 3.3), owing to complications such as the scale height gradient dH/dh, and drifts due to tidal electric fields. In consequence, the index n of equation (24) usually exceeds 0·25.

In the past, many attempts were made to determine q and α from observations during solar eclipses. They proved unsuccessful, because much of the ionizing radiation originates in the solar corona and is not fully cut off by the eclipsing Moon. More reliable data have come from laboratory measurements of recombination coefficients and spacecraft measurements of solar radiation fluxes.

5.3 Sporadic E

Sporadic E, or Es, is a generic term for thin layers of enhanced ionization that occur at around 100–120 km, generally in a rather irregular fashion that is not predictable

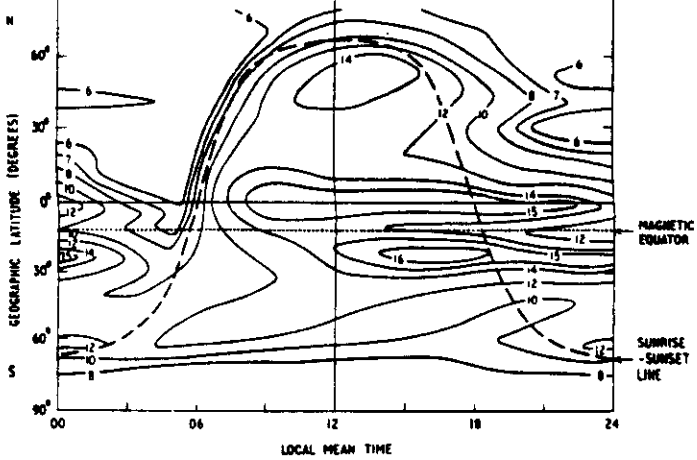

Fig. 13. Prediction map for F2-layer critical frequency, in local time for the American sector, December 1957. (*Courtesy of* Central Radio Propagation Laboratory, US Department of Commerce.)

in detail. They are important in practice because they are often dense enough to affect radio propagation quite seriously. Twelve types of Es have been defined,[14] distinguished by their appearance on ionograms, but in reality there may be only three main physical types:

(a) *Midlatitude Es layers*, sometimes much denser than the normal E layer or even the F2 layer, are thought to be produced by wind shears (small-scale gradients of wind velocity). The sheared wind interacts with the geomagnetic field in such a way as to compress the long-lived metal ions into thin layers, typically 1 km thick but several hundred km in horizontal extent. The wind shears may be associated with large-scale tidal motions, which have a certain regularity, or with smaller-scale winds or gravity waves which have little or no predictability.

(b) *Equatorial Es*, a plasma instability caused by the high electron drift velocity (i.e. the large current density) in the daytime equatorial electrojet (section 4.6).

(c) *Auroral Es* layers are produced by precipitation of keV electrons, particularly during auroral substorms (Section 5.7).

5.4 F1/F2 Splitting

The F1 layer, when observed on ionograms, behaves more or less as a Chapman layer, with an index $n \approx 0{\cdot}2$ in equation (24). As mentioned in Section 4.2, its visibility depends on the ratio $G = \beta^2/\alpha q$ defined by equation (36), the layer being more prominent when G is large—as in summer (β large) and at sunspot minimum (q small)—than when G is small—as in winter (β small) and at sunspot maximum (q large). The matter is really more complex, as F1 layer visibility depends also on the shape of the overlying F2 layer. The appearance of extra F1 stratifications during a solar eclipse is largely due to the decrease of q and consequent increase of G.

5.5 F2 Layer Behaviour

The F2 layer is much less regular, and shows many features that differ from those of a purely solar-controlled layer. Examples may be seen in the world map of Fig. 13, and in Fig. 14 which shows the F2 layer variations at a mid-phenomena are dealt with in Section 6.3.

The shape of the day/night variations of N_mF2 and h_mF2 is largely due to neutral air winds, and to a lesser extent electric fields. Around sunset, the meridional component of the wind changes from equatorward to poleward (see Fig. 6) and the resulting F2 layer drift changes from downward to upward (see Fig. 10). This is a probable cause of the commonly observed increase of N_mF2 in the late evening. The common pre-dawn decrease of N_mF2 is probably connected with the poleward-to-equatorward wind reversal around that time. In detail, these phenomena depend on the geometry of the geomagnetic field, i.e. the dip and declination. For example, when sunrise at the magnetically conjugate point occurs before local sunrise, the inflow of photoelectrons from the opposite hemisphere can produce increases of electron temperature and consequent effects on the electron density.

At night the F2 layer is maintained (a) by being raised by winds (Fig. 10) to heights where the loss coefficient β is small; (b) by inflow from the protonosphere (Section 4.8); (c) by EUV fluxes from the night sky; and perhaps (d) by energetic particles.

The anomalous seasonal variation (Fig. 9) is attributable to changes of the O/N_2 ratio of the neutral air (Section 2.3), which are an indirect consequence of the global circulation in the thermosphere, and which affect the loss coefficient β, and to some extent the production rate q. There is also an annual variation (largely because the variation of Earth-Sun distance modulates the flux of ionizing radiation) and a less well explained semiannual variation, most pronounced in the Southern Hemisphere.

5.6 The Equatorial Ionosphere

Near the geomagnetic equator, the ionosphere shows very anomalous behaviour. The equatorial electrojet in the E layer, and its associated instabilities and Es, has already been mentioned (Section 4.6, 5.3). Its physics seems reasonably well understood, though interesting problems remain, especially about the 'counter-electrojet', an anomalous reversal that occurs on some days, possibly triggered by gravity wave activity.

The main feature of interest in the F2 layer is the daytime 'equatorial trough' or 'Appleton anomaly' (shown in Fig. 13). It is produced by dynamo electric fields, which cause a drift away from the magnetic equator, and disappears at night. At sunset, the F2 layer rises and often develops 'spread F' instabilities, which form plumes extending vertically for several hundred kilometres; Figure 15 shows an extreme example. Evidence from perturbations of satellite orbits has led to the suggestion that the equatorial thermosphere has a prevailing west-to-east motion, which may be attributable to the day-to-night variations of ion drag.

5.7 The High Latitude Ionosphere and the Auroral Ovals

At high latitudes, ionospheric structure is related to the auroral ovals and the magnetosphere, to which the ionosphere is linked by geomagnetic field lines (Section 1.3). Electric currents and energetic particles can flow into the ionosphere, causing heating and consequent upward expansion of the air, which modifies the chemical composition and the thermospheric wind system, with consequent effects on the F layer.

The auroral ovals are the site of the many active phenomena, especially particle precipitation which causes enhanced ionization in all the ionospheric layers. Hartz and Brice[15] defined two types of precipitations: the intense

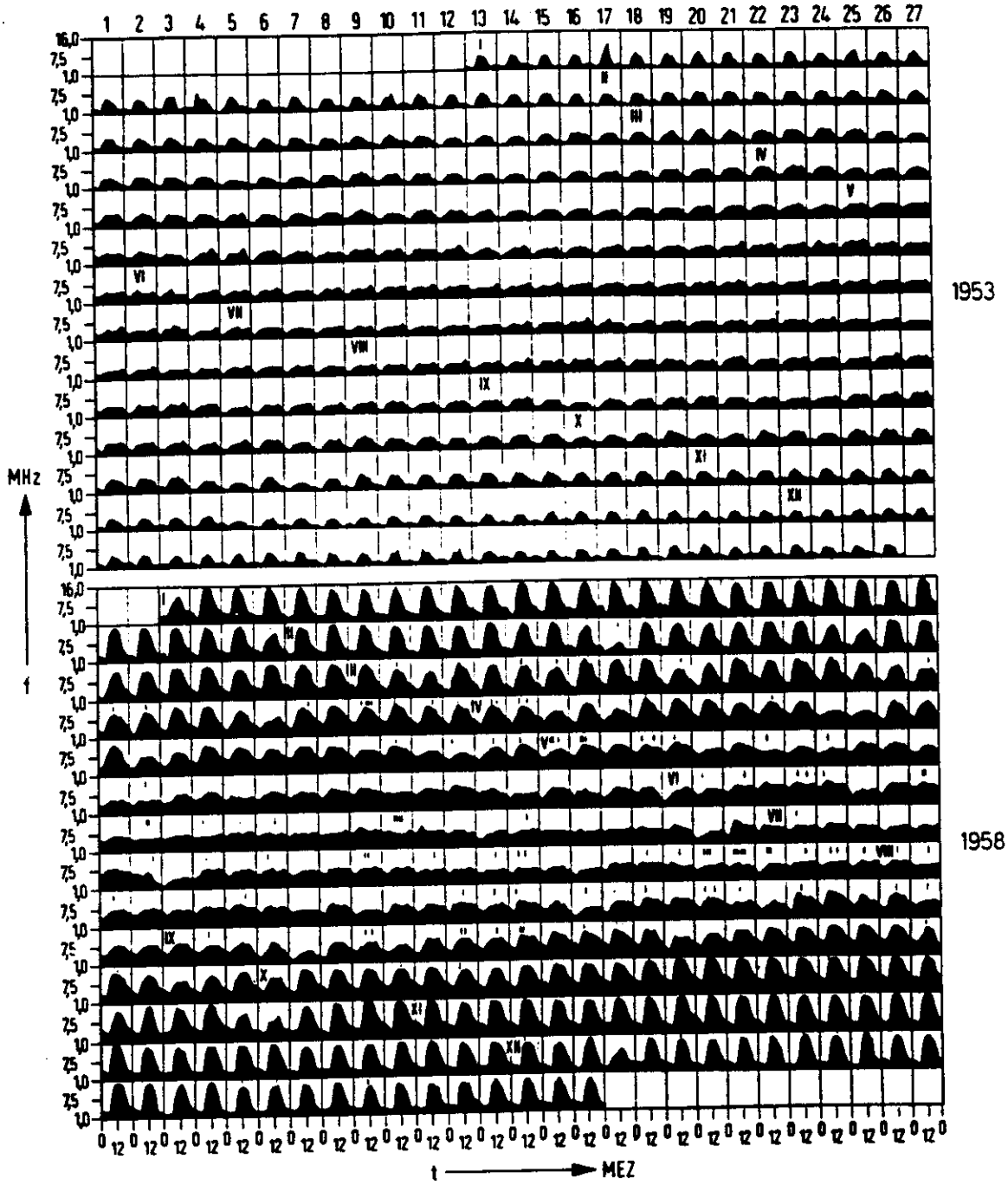

Fig. 14. 'Lindau Mountain Diagrams' showing the critical frequency foF2 at Lindau (Lat. 52°N) throughout the sunspot minimum year 1953 and sunspot maximum year 1958. Each box represents 00–24 LT and 1–16 MHz; the data are arranged in lines of 27 days, to display any recurrences attributable to the solar 27-day rotation period. (*Courtesy of* Max-Planck-Institut für Aeronomie, Katlenburg-Lindau, German Federal Republic.)

impulsive 'splashes' of relatively soft (keV) particles associated with substorms and the auroral oval; and the more persistent background 'drizzle' of harder (MeV) particles at rather lower latitudes. The consequences include:

SPLASH EVENTS
- Discrete auroral forms
- Auroral absorption events
- Auroral sporadic E
- Rapidly fading VHF scatter
- Impulsive Pi pulsations
- Bursts of VLF auroral hiss
- Short bursts of keV electrons
- Bremsstrahlung X-ray bursts
- Spread F echoes
- Negative magnetic bays

DRIZZLE EVENTS
- Steady diffuse aurora
- Slowly varying absorption
- Low diffuse sporadic E
- D layer VHF forward scatter
- Continuous Pc pulsations
- VLF chorus emissions
- Sustained electron fluxes
- Long duration hard X-rays

The actual location of the auroral ovals depends on various geomagnetic and solar-terrestrial parameters. In principle this dependence could be represented either empirically or physically, in the sense explained in Section 1.2. Then the positions of ionospheric features, that are related to the geometry of the auroral oval, could be linked to observable

Fig. 15. The black regions represent small-scale plasma irregularities in the equatorial ionosphere after sunset, as observed by the incoherent scatter radar at Jicamarca, Peru (12°S). The scale size detected by the 50 MHz radar is 3m. (R.F. Woodman, Instituto Geofisico del Peru; from Szuszczewicz, E.P. *et al.*, *Annales Geophysicae*, **6**, p.14, 1988, Gauthier-Villars, Paris.)

solar or interplanetary quantities (possibly with a time delay), with potentialities for either short-term forecasting or long-term prediction.

To this end, Fig. 16 is a schematic plan of the northern auroral oval and features linked to it. The oval can be quite well represented by a circular ring, with its centre offset from the geomagnetic (dip) pole by 2–4 degrees towards the midnight side. The radius and offset depend on the level of geomagnetic activity, which in turn depends on solar activity and the interplanetary magnetic field (IMF). The relation between the geomagnetic latitude Λ of the oval boundaries (degrees), local geomagnetic time GT (in hours) and the geomagnetic Kp index (Section 1.3) is of the type

$$\Lambda = A - B \cos [\pi(GT)/12] \qquad (46)$$

with the following approximate values of the parameters:

Poleward boundary:

$$A = 74 - 0{\cdot}1\ Kp,\ B = 4 - 0{\cdot}5\ Kp \qquad (47)$$

Equatorward boundary:

$$A = 72 - 0{\cdot}9\ Kp,\ B = 5 + 0{\cdot}1\ Kp \qquad (48)$$

The precise formulation of these equations is a matter for debate, since the parameters involved (magnetic latitude, magnetic activity and time) can be defined in different ways. However, equations (47) and (48) do show that the auroral oval thickens and moves equatorward with increasing geomagnetic disturbance.

5.8 The Polar Cap Ionosphere

From early days in ionospheric physics, it was a puzzle as to how the ionosphere was maintained throughout the polar winter in the absence of solar ionizing radiation.

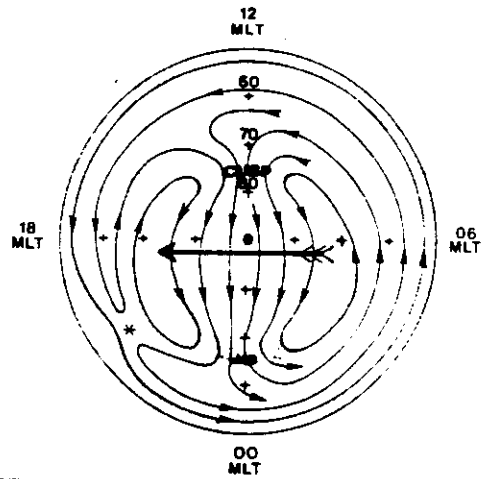

Fig. 16. The auroral oval and associated phenomena. View of the North Polar region, centred on the magnetic pole. The bottom of the diagram represents magnetic midnight, 00 MLT; the top represents magnetic noon, 12 MLT; the outer boundary is at 50° magnetic latitude, the crosses being at magnetic latitudes 80°, 70°, and 60°. The outer ring represents the plasmasphere (mid-latitude ionosphere) which co-rotates with the Earth. The stippled ring represents the approximate location of the hard 'drizzle' precipitation. The inner shaded ring is the auroral oval, showing the approximate locations of the 'cusp' in the noon sector and the Harang discontinuity (HD) near midnight. The fine lines represent typical flow lines of the plasma convection pattern (some curves are left incomplete to reduce congestion); note the stagnation point at 20 MLT. The diagram corresponds roughly to moderate magnetic activity (Kp = 3) with a southward B_z component of the interplanetary magnetic field. (*Courtesy of* S.E.R.C. Rutherford Appleton Laboratory.)

Since the polar caps (within the auroral ovals) are not normally locations of strong particle precipitation, and the night sky provides only weak sources of ionizing radiation, horizontal transport of ionization seemed the most likely solution.

From many observations of plasma motions, by satellite-borne instruments and by coherent and incoherent scatter radar, it is now known that the magnetic linkage between the solar wind, as it sweeps past the Earth, and the geomagnetic field sets up a system of electric fields throughout the high latitude ionosphere.

The resulting $\mathbf{E} \times \mathbf{B}/B^2$ drift, shown in Fig. 16, causes a fast day-to-night flow of plasma across the polar cap. This flow maintains the F2 layer in the dark side of the polar ionosphere, though the supply may be finely balanced because the rapid drift also increases the decay rate of the plasma by increasing the coefficient K'' in equation (37). The drift tends to be faster at times when the south-to-north (B_z) component of the interplanetary magnetic field (IMF) is directed southward (which facilitates linkage between the geomagnetic field and the IMF), and has a more complex pattern when B_z is directed northward.

Recent studies have given new insights into IMF-magnetosphere-ionosphere interactions. As one example of many, Fig. 17 shows ion velocities measured by incoherent scatter radar, a few degrees equatorward of the midday sector of the auroral oval, together with IMF measurements by a satellite. An impulsive increase of velocity and temperature ('flow burst') at 0635 UT— not well resolved in Fig. 17—is thought to result from a sudden magnetic linkage between the magnetosphere and IMF. Later, shortly after a 'southward turning' of the B_z IMF component at 1107 UT, enhanced electric fields and $\mathbf{E} \times \mathbf{B}/B^2$ drift velocity appear in the F region, accompanied by increases of ion temperature attributed to the frictional heating produced by ion-neutral collisions.

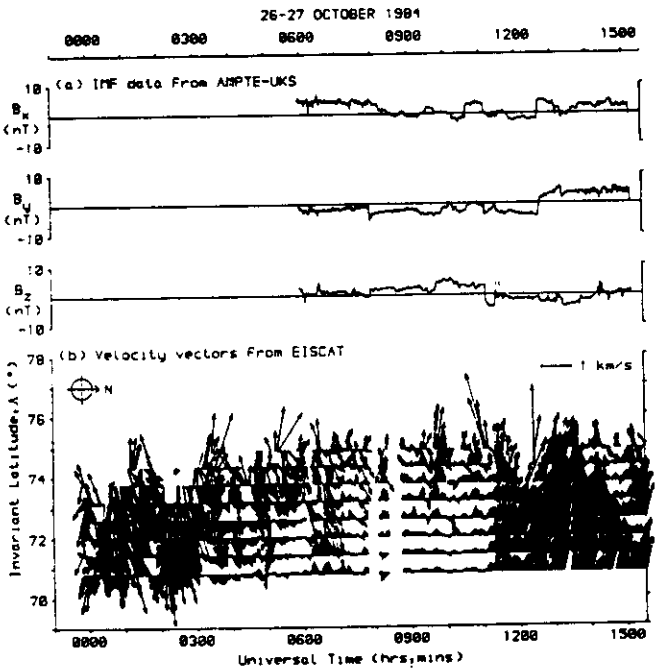

Fig. 17. Plasma velocity vectors at high magnetic latitudes measured by the EISCAT incoherent scatter radar, at a number of latitudes on 27th October 1984. The upper panels show components of the interplanetary magnetic field measured by the AMPTE-UKS satellite situated at a distance of 20 earth radii. (S.E.R.C. Rutherford Appleton Laboratory; from *J. Atmos. Terr. Phys*, 48, p.992, 1986, Pergamon Press, Oxford)

5.9 High Latitude Convection and the Trough

Figure 16 shows that the day-to-night drift in the polar cap is part of a huge high latitude circulation or 'convection'.[16] On the low latitude side of the auroral oval, this convection gives rise to the 'ionospheric trough', a region of low plasma density originally discovered by satellites. The combination of the Earth's rotation and the convection velocity causes plasma to become almost stationary in the evening sector of the trough, as shown in Fig. 16. If this region of stagnation is in darkness, the ion density can decay to very low levels. The 'drizzle' precipitation often produces small-scale irregular structure and strong airglow emission in the trough region.

The equatorward boundary of the trough is linked to the plasmapause, which is the boundary between the inner magnetosphere that rotates with the Earth (and is magnetically linked to the ionosphere at mid- and low latitudes) and the more tenuous outer magnetosphere, that does not rotate with the Earth.[17]

6 Solar–Terrestrial Relationships and Ionospheric Storms

6.1 Solar Flares and Sudden Ionospheric Disturbances

The intense X-rays from solar flares produce strong enhancements of electron density in the D layer, giving rise to 'sudden ionospheric disturbances' (SID). These embrace several phenomena, including radio short-wave 'fade-outs', effects on LF/VLF propagation, and magnetic perturbations, which occur only in the sunlit hemisphere and typically last for half an hour. Soon after, MeV particles arrive, causing enhanced radio wave absorption at high latitudes (polar cap absorption, PCA).

6.2 Geomagnetic Storms

The streams of low energy plasma liberated from solar disturbances, especially from the vicinity of solar flares, travel outwards in the solar wind (which becomes faster and denser), taking 24 hours or so to reach the Earth. A stream's impact on the magnetosphere causes a 'magnetic storm', which often starts with a compression of the geomagnetic field, observed at the ground as a 'storm sudden commencement' (SSC). The ensuing complicated interaction of the plasma stream and the magnetosphere has several consequences, including the establishment of a 'ring current' around the Earth (largely carried by keV ions). The ring current causes the storm-time decrease of the geomagnetic field, which is greatest at 12–24 hours after the SSC and then decays in 2–3 days. The auroral oval expands equatorward during storms (Section 5.7), and the plasmapause and trough (Section 5.9) also move to lower latitudes than normal.

6.3 Ionospheric Storms

During a geomagnetic storm, particle precipitation at high latitudes produces disturbances at D layer heights, probably chemical in nature (e.g. through the production of extra NO). The effects are propagated to the mid-latitude D layer, where they may last for ten days or so. Figure 18 gives examples (not necessarily typical) of storm effects at mid-latitudes; there are marked effects in the F2 and D layers, but not in the E layer.

The F2 layer is often profoundly affected during magnetic storms, with severe effects on radio propagation. At mid-latitudes the F2 layer electron density initially increases, then often decreases during the storm's main phase, and recovers in 2–3 days. Examples of these 'negative storm effects' can be seen in Fig. 14. In winter, however, there is often a 'positive' effect, i.e. an increase of F2 layer density in the main phase. 'Positive' F2 layer effects are quite common at low latitudes.

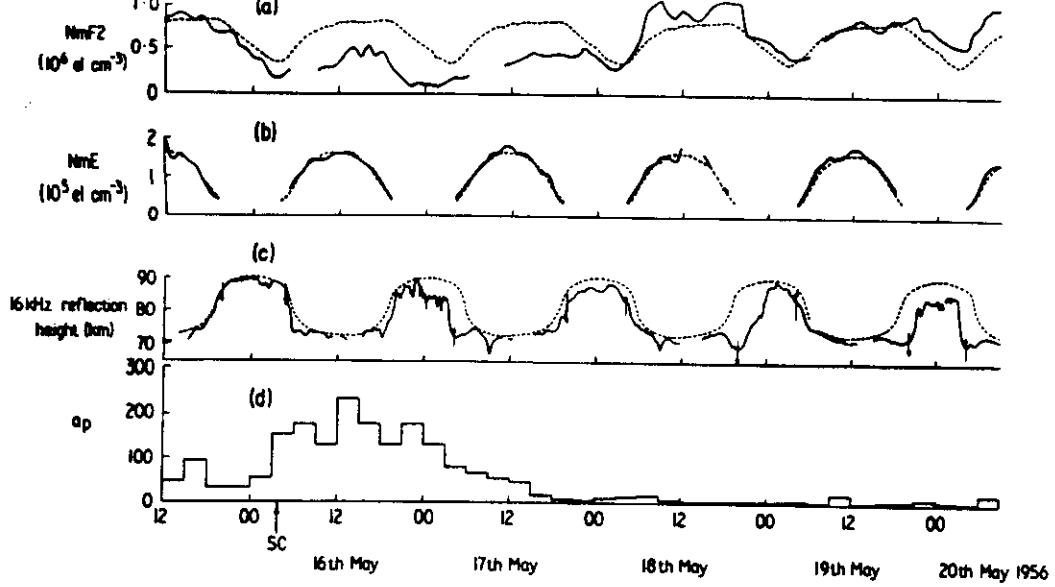

Fig. 18. Storm effects observed at Slough, May 1956, in the D, E and F2 layers, together with the index a_p which measures the degree of geomagnetic disturbance. The F2 layer shows both 'positive' and 'negative' effects (increases and decreases of N_mF2. The E layer is relatively undisturbed, but there are pronounced changes in the D layer, as shown by the effects on the reflection height of 16 kHz transmissions. (L. Thomas, in 'The Radiating Atmosphere', ed. B.M. McCormac (D. Reidel, Dordrecht, 1971))

These storm effects, which vary in time and location in a complicated manner, seem to originate from the energy inputs (joule heating and particles) at high latitudes, which generate winds and waves that spread globally. Thermospheric composition changes, electric fields and particle precipitation all play a part. The mechanisms involved are still far from clear, but there must be a 'storm circulation' (somewhat as sketched in Fig. 19) superimposed on the quiet day wind system described in Section 2.4. The equatorward winds of the storm circulation cause some lifting of the F2 layer, which affects N_mF2 in the way shown in Fig. 10. The 'negative' storm effects at mid-latitudes are almost certainly due to neutral composition changes (i.e. increase of the neutral $[N_2/O]$ ratio) which increase the loss coefficient β and decrease N_m, as given by equation (44). The question of whether such composition changes can really be conveyed by winds and waves from the auroral oval is still under study.[18] Alternatively, these effects might perhaps be due to localized particle precipitation, which is known to produce depletions of N_mF2, and strong airglow emission in the trough region. The 'positive' F2 layer storm effects in winter, and at low latitudes, may be due to *decreases* of $[N_2/O]$ ratio.

7 Conclusion

7.1 Progress in Recent Years

Ionospheric science nowadays has several aspects. First, it is an old but still active branch of the domain of solar-terrestrial physics; experimental and theoretical studies of the ionosphere have contributed enormously to understanding of the Earth's environment. Second, it contributes to the science and technology of radio communications; the practical use of the ionosphere for communications is still great, and could be improved by further progress in the challenging field of 'predicting and forecasting'. Third, the mathematical subject of wave propagation in the ionosphere deals with waves of many types; besides man-made radio transmissions, a vast range of electromagnetic emissions, magnetic pulsations and other phenomena originate in the ionosphere, or travel through it. Fourth, the ionosphere offers great scope for plasma physics, both experimental and theoretical.

The recent developments mentioned in this paper are mostly concerned with the first aspect (although, in time, progress in scientific understanding generally leads to practical benefits). The advances have come about through new instrumentation—both ground-based and in space—offering better spatial and temporal resolution and ever-increasing data rates. On the theoretical side, much of the recent progress in understanding the ionosphere has come from theoretical modelling. Modern computers have made possible the solving of the basic equations (1)–(3), for the

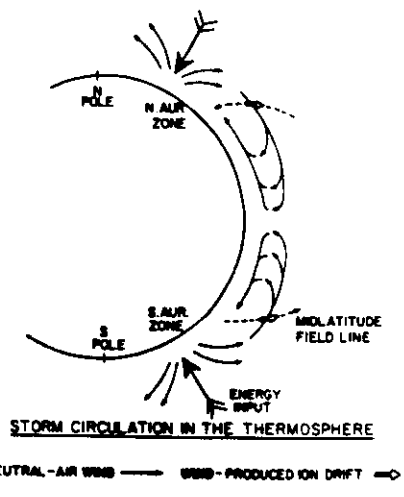

Fig. 19. Idealized sketch of the thermospheric 'storm circulation'. The auroral heating drives strong equatorward winds at mid-latitudes, which affect the F2 layer ionization by driving it along geomagnetic field lines (white arrows). The return circulation, envisaged to be below 150 km, is speculative, as are the winds blowing into the polar cap. (From *Radio Sci.*, 9, p. 185, 1974, American Geophysical Union.)

ions, electrons and neutral gases, with ever-increasing realism. Such work has yielded a good picture of the general thermospheric circulation (Section 2.4), and of the way it produces the daily and seasonal variations described in Section 5.5 (whether chemical or dynamical in origin), and has made notable progress towards understanding ionospheric storms. There remain many questions about the thermosphere, such as the roles of the various energy sources: solar EUV radiation; particles and currents from the magnetosphere and solar wind; and tidal and wave energy propagated from below.

The real problems remain at the boundaries, both above and below; i.e. the interactions with the lower atmosphere and the magnetosphere. The latter embraces the whole question of the effect of geomagnetic disturbance and of the interplanetary magnetic field, primarily at high latitudes, but also how the effects spread world-wide. Several topics and ideas within this theme have been mentioned in Sections 5.7–5.9 and 6.3.

Influences of the lower atmosphere on the ionosphere remain a subject for much present and future study. That the lower atmosphere, with its huge mass and energy density, should affect the upper atmosphere is hardly surprising. It has long been known that some tidal components and oscillations (Section 2.5) are excited low in the atmosphere, and that some gravity waves (Section 2.6) originate in storms and explosions, and possibly earthquakes. The large electric fields generated in thunderstorms can affect the electrodynamics of the ionosphere. There have been intriguing suggestions of topographic influences on the ionosphere.[19,20]

Although this paper has concentrated on the large-scale structure of the ionosphere, there exists detailed structure possessing a wide range of scale size. The small-scale irregularities at auroral and equatorial latitudes are interesting examples of plasma instability phenomena, but there is a wide range of irregular structure that causes radio wave fading, and scintillation of radio signals traversing the ionosphere, of which spread F and sporadic E are examples. Medium-scale structure, 10–1000 km in scale, is widely observed but not well explained.

As a natural plasma, often non-linear and non-thermal in its behaviour, the ionosphere provides a site for many kinds of active experiments with radio waves, powerful enough to produce observable 'ionospheric modifications' (heating and plasma instabilities), and with chemical releases and particle beam experiments. Such experiments provide novel physical and chemical insights, though they often raise as many questions as they solve.

7.2 The Frontiers: Major Areas of Active Research

This paper has tried to review the basic physics of the ionosphere. The account is highly simplified and avoids many questions and complexities. The basic mechanisms of the ionosphere seem to be known, but there are many topical questions still to be solved in this active area of science. The frontiers include:

(1) The detailed analysis of the thermospheric circulation.
(2) Influences of the magnetosphere, IMF and the solar wind.
(3) Influences of oceans, mountains, earthquakes, thunderstorms.
(4) Mechanisms of ionospheric storms.
(5) The cause of irregular structure of a wide variety of scales.
(6) Active experiments: the ionosphere as a physics/chemistry laboratory.
(7) Predictability of the ionosphere on various time-scales.

For future progress, new experimental facilities will be needed, and will bring new opportunities—and new puzzles to solve. More powerful computers will enhance data handling and enable more demanding theoretical projects to be tackled, but the basic everyday monitoring of this important part of the environment—spanning five solar cycles since 1931—will be as vital for progress in the future as it has been in the past.

8 Acknowledgments

This paper is a considerably expanded version of the notes of a lecture, presented at the IEE Vacation School on Radio Propagation, September 1986, and published in a book (M. P. M. Hall and L. W. Barclay, editors) by Peter Peregrinus, 1988.

9 Bibliography

Ratcliffe, J. A., 'Sun, Earth, and Radio' (World University Library, 1970).
Rishbeth, H. and Garriott, O. K., 'Introduction to Ionospheric Physics' (Academic Press, New York, 1969).
Hargreaves, J. K., 'The Upper Atmosphere and Solar-Terrestrial Relations' (Van Nostrand-Reinhold, New York, 1979).
Giraud, A. and Petit, M. 'Ionospheric Techniques and Phenomena' (Reidel, Dordrecht, 1978).
Whitten, R. C. and Poppoff, I. G. 'Introduction to Aeronomy' (Wiley, New York, 1971).
Banks, P. R. and Kockarts, G. 'Aeronomy', (2 vols) (Academic Press, New York, 1973).
Jursa, A. S. 'Handbook of Geophysics and the Space Environment' (Air Force Geophysics Laboratory, Bedford Mass., USA, 1985).

10 References

1 Appleton, E. V. and Barnett, M. A. F., 'Local reflection of wireless waves from the upper atmosphere', *Nature*, 115, pp. 333–4, 1925.
2 Breit, G. and Tuve, M. A., 'A radio method of estimating the height of the conducting layer', *Nature*, 116, p. 357, 1925.
3 Gordon, W. E., 'Electromagnetic probing of the ionosphere', *J. Atmos. Terr. Phys*, 32, pp. 459–66, 1970, and subsequent articles in the same issue.
4 Ratcliffe, J. A. (Ed.), 'Fifty years of the ionosphere', *J. Atmos. Terr. Phys*, 36, pp. 2069–320, 1974.
5 Evans, J. V., 'Theory and practice of ionosphere study by Thomson scatter radar', *Proc. IEEE*, 57, pp. 496–530, 1969.
6 Lindzen, R. S. and Chapman, S., 'Atmospheric tides', *Space Sci. Rev.*, 10, p. 3–188, 1969.
7 Beer, T., 'Atmospheric Waves' (Adam Hilger, London, 1974).
8 Allen, C. W., 'The interpretation of the XUV solar spectrum', *Space Sci. Rev.*, 4, pp. 91–122, 1965.
9 Torr, D. G. and Torr, M. R., 'Chemistry of the ionosphere and thermosphere', *J. Atmos. Terr. Phys*, 40, pp. 797–839, 1979.
10 Rishbeth, H., 'On the continuity equation of the F2-layer', *J. Atmos. Terr. Phys*, 48, pp. 511–9, 1986.
11 Dougherty, J. P., 'On the influence of horizontal motion of the neutral air on the difusion equation of the F region', *J. Atmos. Terr. Phys*, 20, pp. 167–176, 1961.
12 Moore, T. E., 'Superthermal ionospheric outflows', *Rev. Geophys. Space Phys*, 22, pp. 264–74, 1984.
13 Thomas, L., 'The summer to winter changes in the D-region and stratosphere', *J. Atmos. Terr. Phys*, 37, pp. 595–600, 1975.
14 Piggott, W. R., and Rawer, K., 'URSI handbook of ionogram interpretation and reduction', UAG-23, World Data Centre A. Boulder, Colo., US Department of Commerce, 1972.
15 Hartz, T. R. and Brice, N. M., 'The general pattern of auroral particle precipitation', *Planet. Space Sci.*, 15, pp. 301–29, 1967.
16 Knudsen, W. C., 'Magnetospheric convection and the high-latitude F2 ionosphere', *J. Geophys. Res.*, 79, pp. 1046–55, 1974.
17 Carpenter, D. L. and Park, C. G., 'On what ionosphere workers should know about the plasmapause-plasmasphere', *Rev. Geophys. Space Phys*, 11, pp. 133–54, 1973.
18 Rishbeth, H., Fuller-Rowell, T. J. and Rodger, A. S., 'F-layer storms and thermospheric composition', *Physica Scripta*, 36, pp. 327–36, 1987.
19 Balsley, B. B., 'E region dynamics', *J. Atmos. Terr. Phys*, 39, pp. 1087–96, 1977.
20 Watanabe, S. and Oya, H., 'Occurrence characteristics of low latitude ionospheric irregularities observed by impedance probe on board the Hinotori satellite', *J. Geomagn. Geoelect.*, 38, pp. 125–49, 1986.

Manuscript received by the Institution in final form on 7th July 1988
Paper No. 2387/COMM481